ELSEVIER

Nuclear Instruments and Methods in Physics Research A 479 (2002) 439–455

NUCLEAR INSTRUMENTS & METHODS IN PHYSICS RESEARCH Section A

www.elsevier.com/locate/nima

The optical module for the NESTOR neutrino telescope

E.G. Anassontzis[a], P. Ioannou[a], S. Katsanevas[a], Ch. Kourkoumelis[a], J. McNutt[a], A. Manousakis-Katsikakis[a], L. Moraitis[a], L.K. Resvanis[a], S.A. Sotiriou[a,*], V. Tsagli[a], G. Voulgaris[a], I. Siotis[b], G. Fanourakis[c], G. Grammatikakis[c], A.E. Ball[d], S. Bottai[e], A. Cartacci[e], B. Monteleoni[e,✠], U. Keusen[f], P. Koske[f], V.A. Zhukov[g], V.K. Rucol[h,✠], V.V. Ledenev[i]

[a] *Physics Laboratory, University of Athens, Greece*
[b] *NCRC "DEMOKRITOS", Greece*
[c] *University of Crete, Greece*
[d] *CERN, Switzerland*
[e] *University of Florence, Italy*
[f] *University of Kiel, Germany*
[g] *Institute for Nuclear Research, Russian Academy of Sciences, Russia*
[h] *Institute of Oceanology, Russian Academy of Sciences, Russia*
[i] *Experimental Design Bureau of Oceanological Equipment, Russian Academy of Sciences, Russia*

The NESTOR collaboration

Received 24 October 2000; received in revised form 12 February 2001; accepted 19 March 2001

Abstract

NESTOR is a deep-sea water Cherenkov neutrino detector now under construction for deployment in the Mediterranean off Greece. Its key component is an optical module employing a photomultiplier tube with a 15 in. hemispherical photocathode in a transparent glass pressure housing. Extensive tests have been made on the sensitivity, uniformity, time resolution, noise rates and mechanical properties of the module: several test deployments have been made at sea.

Keywords: Neutrino telescope; Cherenkov detector; Optical sensor

1. Introduction

NESTOR[1] [1–4] is a deep-sea neutrino telescope which is being deployed in the Mediterranean off the South–West coast of the Peleponnese in Greece. Neutrinos, when they interact in the earth

*Corresponding author. Ellinogermaniki Agogi S.A., Head of the Research and Development Dept., D. Plakentias Ave. 25, GR-15344 Chalandri, Greece. Tel.: +30-16853-220; fax: +30-16821-953.

E-mail address: sotiriou@ellinogermaniki.gr (S.A. Sotiriou).

✠ Deceased.

[1] NESTOR—Neutrino Experimental Submarine Telescope with Oceanological Research.

0168-9002/02/$ - see front matter
PII: S0168-9002(01)00927-5

below or in the seawater around the detector, produce muons which can be observed by the Cherenkov radiation they emit. At an operating depth of more than 3500 m, the detector is effectively shielded from low energy muons produced in atmospheric interactions.

A full NESTOR tower will consist of 168 optical modules fixed on a semi-rigid structure which ensures good geometrical location: this is important in order to reconstruct the interaction point and direction of the incoming neutrinos. The key element, the optical module, is a light sensor with good single photoelectron resolution and spectral response from 300–650 nm, which is capable of operating in the sea at depths of up to 6700 m.

After a brief review of the site characteristics and the overall detector concept, a detailed description of the design, construction, development and testing of the optical modules is given.

2. Site characteristics

The major feature of the sea floor in the Ionian Sea is the Eastern Mediterranean Ridge, a high submarine mountain chain, which extends in a south-easterly direction from southern Italy and then turns eastward, south of Crete, towards Cyprus. Between this range and the western coast of the Peleponnese is the Hellenic Trench, the deepest part of the Mediterranean, which in places exceeds 5000 m: because of the sea bottom morphology the area is protected from major deep water perturbations.

Surveys, carried out in 1991 and 1992 jointly with oceanographic teams from the Russian Academy of Sciences, located a broad plateau some 8 km × 9 km in area on the eastern side of the Hellenic Trench: this plateau has a mean depth of 3800 m which is constant to within ±50 m over its entire area [3–6].

The center of the plateau[2] is only 7.5 nautical miles from the island of Sapienza and 11 nautical miles from the town of Methoni on the south-western tip of the Peleponnese mainland. Detectors deployed in this area can therefore be connected to shore by modest lengths of electro-optical cable.

Measurements made at the site since 1992 show very clear water with a transmissivity of 55 ± 10 m at 460 nm wavelength [6], water current velocities consistently below 10 cm/s and water temperatures of 14°C with little variation throughout the year [7].

Extensive core samples of the sea bottom sediments over the site have been analysed; with a mean density of 1.5 g/cm^3, they indicate a slow accumulation rate of 7–18 cm over 10 000 years giving a firm clay deposit for good anchoring. There is no evidence of any submarine rock falls [7,8].

In November 1994, a side-scan sonar and air pressure gun were used to survey the site area and the cable route to Methoni: maps of the sea bottom were produced to a scale of 1 : 10 000 using differential GPS for position location [8].

The optical background due to ^{40}K decay was measured to be 75 kHz/OM at the quarter photoelectron level. Intermittent bursts of 3–5 s duration are also detected and occupy around 1% of the active time: these are consistent with bioluminescent activity [9,10].

3. The detector

The basic element of the NESTOR detector is a hexagonal floor or star of 32 m diameter. A central casing supports a 1 m diameter spherical titanium pressure housing which contains the data acquisition electronics, power converters, monitoring, control and data transmission equipment.

Attached to the central casing are six arms built from titanium tubes to form a lightweight but rigid lattice girder structure. The girder elements are of 5 m modular length: normally three elements are used per arm but the modular construction allows for different detector configurations if required: the arms can also be folded for transport and deployment. A number of structures have also been made from sea-resistant aluminum alloy.

Two optical modules (OM) are installed at the end of each arm, one facing upwards and the other

[2] Site coordinates: 36° 37.5′N, 21° 34.6′E.

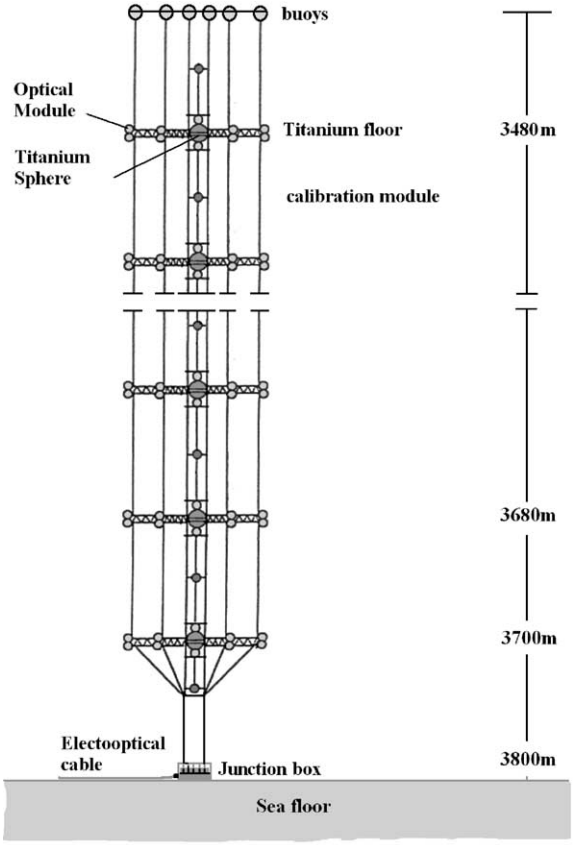

Fig. 1. The NESTOR neutrino telescope.

downwards: OMs are also installed above and below the central casing making a total of 14 per floor. Using the OMs in pairs gives 4π coverage, enhances the discrimination between upward and downward going particles and improves the background rejection.

A full NESTOR tower (Fig. 1) will consist of 12 such floors, spaced vertically by 20–30 m: small LED modules will be installed between floors for OM calibration. The gain and the timing characteristics of the OMs will be monitored continuously by LEDs placed halfway between floors. The optical characteristics of the NESTOR site allow the simultaneous cross calibration of the OMs of many floors using the same LED. The floors are connected to a sea bottom unit, which contains the anchor and its release mechanism, the junction box/fan-out for the electro-optical cable from shore and a number of environmental monitoring packages. Connections of the electro-optical cables, the shore cable to the junction box and the cables from the junction box to each titanium sphere, are all made at the surface during deployment. This avoids the use of deep submersible vehicles and wet-mating connections. Eventually a number of such towers could be deployed to form a very large neutrino telescope.

4. The NESTOR optical module

The OM (Fig. 2) consists of a 15 in. diameter photomultiplier tube (PMT) installed in a spherical glass pressure housing of 400 mm nominal inside diameter: this 'Benthos' sphere, made of two hemispheres with a ground glass interface, can withstand the high external pressures ($\sim$400 Atm) at operating depths. Optical coupling between the glass envelope of the PMT and the sphere is achieved by using a silicone gel or glycerine.

Within the pressure sphere, each PMT is surrounded by a high permeability magnetic shield in the form of a μ-metal cage to reduce the effects of the Earth's geomagnetic field inside the PMT [10,11]. The HV power for the PMT is generated locally by a dc–dc converter, mounted on an aluminum disk, which also acts as a heat sink.

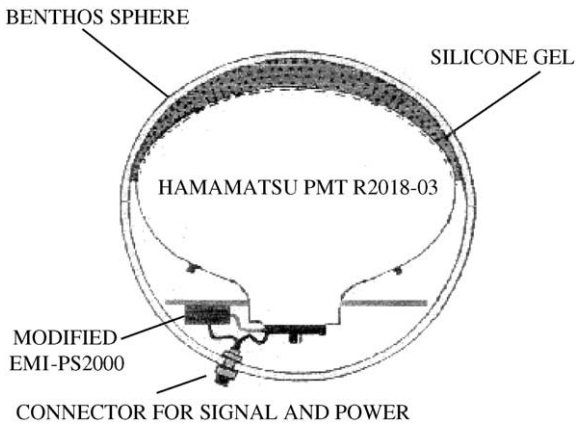

Fig. 2. Cross-sectional view of the OM with the PMT facing upward.

Connection to the OM is through a single, high pressure, 7 pin electrical connector: it is clearly important to keep the number of holes in the glass pressure sphere to a minimum. The connector carries the PMT signal, as well as the low voltage supply, control and monitoring lines. Each OM is connected to the central Ti electronics sphere by a hybrid (twisted pairs and co-axial) cable.

In the following sections, the components of the NESTOR OM are described in detail.

4.1. The Hamamatsu PMT R2018-03

The lifetime and success of a deep underwater detector like NESTOR depends strongly on the quality and proper operation of its PMTs. For such a detector, the PMTs employed must meet the following requirements:

- Large photocathode area.
- High quantum efficiency of the photocathode. The higher the quantum efficiency, the higher the detection efficiency which results in a larger active volume, a higher reconstruction efficiency and a lower energy threshold.
- Large angular coverage. The design of the NESTOR detector uses omni-directional combinations consisting of two back to back OMs. Each OM should cover efficiently the volume around it. It is therefore crucial to use a PMT with large photocathode area having uniform response over its surface.
- Good timing response, which will allow precise reconstruction of the muon track.
- Good pulse height resolution: events far from the detector may only illuminate the PMT at the single photoelectron level.
- Small dark count rate so that the events due to noise hits will not dominate the online processing system.
- Good linearity over a large dynamic range, from one photoelectron to approximately 100 photoelectrons.
- Long time stability in gain.

After considering all the commercially available large area PMTs, the 15 in. PMT manufactured by Hamamatsu Photonics Co, Hamamatsu, Japan (type R2018-03) was selected.

Table 1
The manufacturer's specifications of the PMT R2018-03

Type	Hamamatsu R2018-03
Bulb material	Borosilicate glass
Photocathode diameter	15 in (382 mm)
Spectral sensitivity	300–500 nm
Number of stage	13
Gain (op. Voltage)	5×10^7
Quantum efficiency	20% (410 ± 30 nm)
Peak to valley ratio	1.2
TT jitter at 1 pe	7 ns
Rate (th. 0.25 pe, 25°C)	<40 kHz

The specifications of the PMT R2018-03 are presented in Table 1.

It is of similar construction to the 20 in. PMT used in Super Kamiokande but the 20 in. version will not fit into a standard glass pressure housing. The PMT R2018-03 performance has been improved significantly compared to the earlier version R2018, used in DUMAND [12–14].

The photocathode shape has changed from hemispherical to an oblate ellipsoid by revolution in order to improve the time jitter of the PMT. The Venetian blind structure has changed from one-slat to two-slat structure in order to reduce the number of photoelectrons missing the first dynode. Finally three focusing grids were added between the photocathode and the first dynode in order to achieve a further reduction of the time jitter, FWHM ≈ 7 ns, at the single photoelectron level. The resistive chain of the PMT R2018-03 is shown in detail in Fig. 3. The typical value for the peak to valley ratio of the single photoelectron pulse-height distribution is 1.2. The photocathode measures 372 mm in diameter: it is coated with a bialkali compound (Sb–K–Cs) which has high spectral sensitivity for blue light, spectral response extending from 300 to 650 nm, low thermionic emission, and operating voltage lower than 2500 V with a typical gain of 5×10^7.

The typical quantum efficiency of the PMT is 20%, while the collection efficiency is about 65%–70% [10]. The dark count rate at the voltage required for a gain of 5×10^7 is less than 10 kHz at 25°C for 30 mV discriminator threshold.

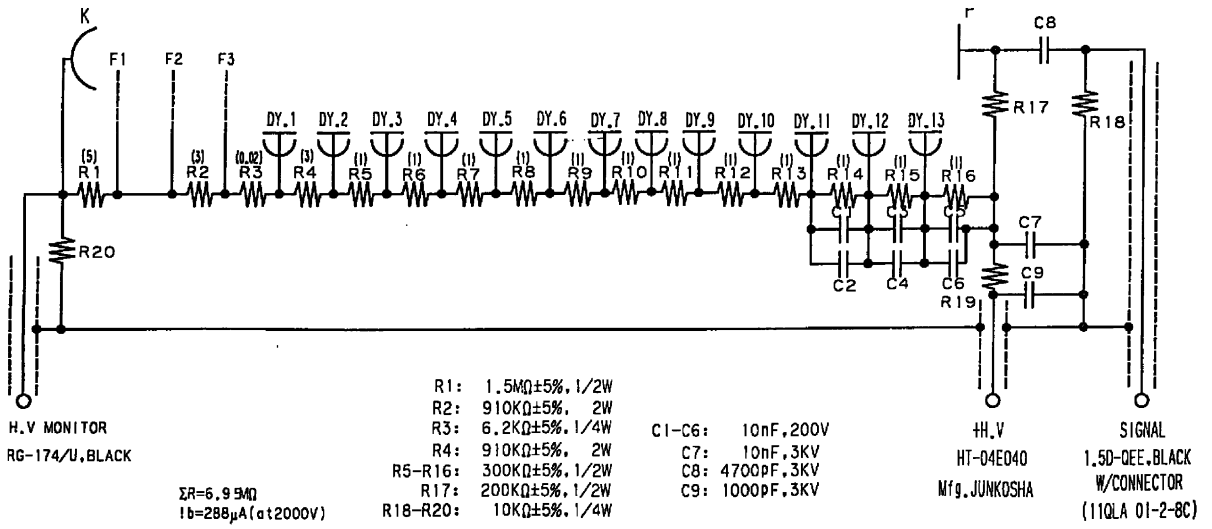

Fig. 3. The bleeder string of the PMT R2018-03 by Hamamatsu Photonics Co.

4.2. The glass housing 2040–17V

The glass housing (Benthos Inc, North Falmouth, MA, USA, type 2040–17 V) consists of two hemispheres of annealed, low expansion borosilicate glass; the equatorial surfaces are carefully ground to match each other. The glass has very good optical transmission for $\lambda > 350$ nm (see Fig. 4) with a refractive index of 1.47 [15].

Each complete housing is tested by the manufacturer at 700 Atm with three pressure cycles of at least 15 min duration. It is rated for a continuous external pressure of 670 Atm. At atmospheric pressure the sphere has a nominal outer diameter of 430 mm and a wall thickness of 14 mm: at the operating depth of 3800 m the diameter contracts by 2.45 mm [10].

The single electrical connector requires a precision drilled hole in the glass hemisphere at 25° from the pole. A 7 pin receptacle (series 35, type 2) from GISMA GMBH is used: this connector is designed for deep-sea applications and has a Ti external housing. Prior to mounting, each receptacle is tested at 550 Atm, open faced (without connected plug) for at least 12 h. After the connector is fitted the empty glass housing is pressure tested at 600 Atm for 24 h.

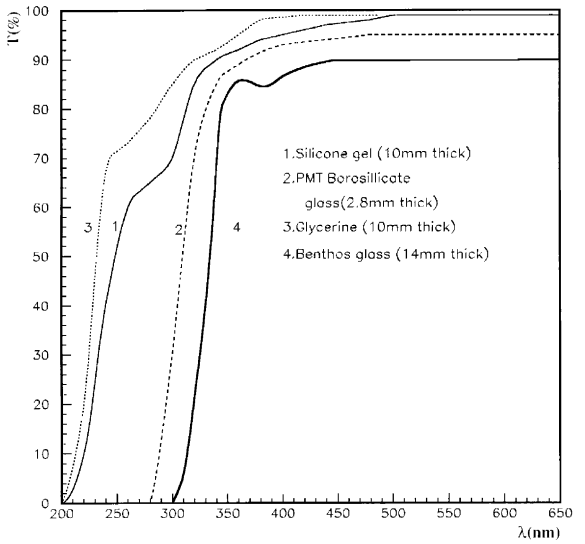

Fig. 4. The transparencies of the silicon gel (1), of the PMT glass (2), and of the glycerin (3). Glycerin is more transparent than the silicon gel. The transparency of the glass housing as a function of wavelength (Benthos Inc., type 2040–17 V) is also shown (4).

4.3. The μ-metal cage

In a large PMT, the velocities of photoelectrons near the photo-cathode are relatively low and their

direction can be influenced by external magnetic fields. It is therefore important to ensure that the magnetic field inside the tube is low and uniform.

To reduce the effects of the Earth's geomagnetic field, the PMT is surrounded by a high permeability screen in the form of cage made from μ-metal wire: the design was based on cages made by Tohuku University, Sendai, Japan for the DUMAND neutrino telescope [12]. Clearly there is a compromise between effectiveness of the screen and the area of the photocathode, which is shaded by it. Following simulations at NCRC Demokritos, Athens the NESTOR field cages were designed using 0.8 mm diameter μ-metal wire, in a nominal square grid, with a wire spacing of 17 mm: this gives about 8% shading of the photo-cathode area. The cages are spot welded together over hard wood moulds as two hemispheres and then annealed at 1070°C for 1 h in a vacuum oven. Field mapping of prototypes produced at CERN, using a Hall effect magnetometer with a resolution of $\pm 0.1\,\mu$T, showed that the field inside the cage is reduced to 12% of the geomagnetic field with a field uniformity of $\pm 0.8\,\mu$T.

In the assembly of the optical module, care is taken to ensure that the spacing between the grid and the glass envelope of the PMT is at least 4 mm over the photo-cathode area, thus reducing any local field perturbations very close to the wires.

4.4. Optical coupling

In order to provide good optical coupling between the glass envelope of the PMT and the Benthos sphere, the PMT and the μ-metal cage are fixed inside the glass housing using optically transparent silicone gel. This provides support to the PMT but is still sufficiently elastic to protect it from possible damage due to the compression of the Benthos sphere in the deep sea. The refractive index of the gel is 1.403, which is close to that of the glass [10].

The gel has good optical transmission properties down to 250 nm (Fig. 4) and matches well the rest of the transparent optical material used namely the PMT borosilicate glass envelope and the Benthos glass.

A disadvantage of using silicone gel is that the PMT and μ-metal cage are difficult to extract from the Benthos sphere in case of malfunction. An alternative, used now in all recent versions of the OMs, is to use purified glycerine for the optical coupling [10]. Glycerine was first used by the INR-NESTOR group as early as 1989 [16]. The refractive index of 1.478 is even closer to that of the glass and the transparency is some 8% better than gel (Fig. 4). As the glycerine remains liquid it has to be sealed in the Benthos sphere by a 6 cm thick gel gasket: this is floated on the surface of the glycerine during assembly. The glycerine technique is also applied by the BAIKAL group [17–19]. In the case of BAIKAL Optical module the gasket that supports the Optical module consists from polyurethane. Long series of tests have been performed in a hyperbaric chamber and in the ocean at 4000 m depth showing that the gel gasket can support sufficiently the glycerine in the case of upward looking modules.

Fig. 5 shows the mechanical setup used for the assembling of the PMT inside the glass hemisphere. The PMT (with the μ-metal cage) is fixed to an adjustable support frame, which allows the positioning of the PMT, with an accuracy of 1 mm, inside the glass hemisphere. The gel is produced by

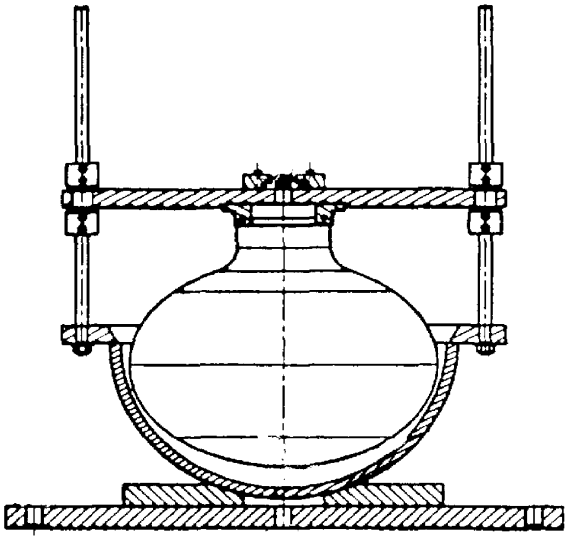

Fig. 5. The mechanical setup for the assembling of the PMT inside the glass housing.

mixing its two components and then poured inside the hemisphere or over the glycerine: it takes about 30 h for the gel to polymerize. About 3.5 kg of gel are needed for a full filling and 0.5 kg for the gasket only.

Both procedures has been shown to be effective in the sea trials.

4.5. The HV power supply

To avoid high voltage on cables in the water, the high voltage (HV) supply for the PMT is generated within the OM. The unit, which is supplied with 24 V dc, is an adjustable dc–dc converter-PS2000—manufactured and modified by THORN-EMI to give an output voltage up to 2500 V dc. Its specification is as follows:

- Input voltage $+24$ V dc $\pm 10\%$.
- Input current 350 mA at 24 V dc.
- Fully adjustable output voltage 50–2500 V.
- Output current 0–1 mA.

The output ripple is quoted at less than 20 mV, peak to peak, between 1 and 100 kHz at operating temperatures in the range 0–50°C. Measured short term stability (in any 10 min period) is better than 0.2%.

The output voltage is set externally by a voltage level of 0–10 V applied to the control pins, and can be monitored via a $\div 1000$ divider within the unit. These signals, together with the 24 V supply and PMT signal, are routed via the 7 pin GISMA connector.

All units have been tested extensively under static load. Some were connected to a PMT for at least 2 years before they are used in the sea. The manufacturer's estimate of the mean time between failure (MTBF) is 300 000 h: Present tests give a measured lower limit of more than 50 000 h (6 years) [1].

4.6. Data transfer

Each OM is connected by copper cable to the central titanium sphere of its floor which contains the control/monitoring and data transmission systems.

In early tests (deployments between 1996–1997), hybrid cables were not available and both signal and power for the PMT's were carried on a 50 Ω coaxial cable. In these tests, the signal was ac coupled to the cable and a filter added to cut out noise induced on the power line from the HV supply. The HV value was preset by using a resistive divider in the input power line: the HV control and monitoring lines on the dc–dc converter could not be used. The HV supply and divider were mounted on an aluminum disk (heat sink) supported around the neck of the PMT (Fig. 6).

The present configuration uses a hybrid cable from each OM to the central sphere: this contains a 50 Ω coaxial cable for the PMT signal and four isolated wires for the 24 V supply, dc–dc converter control voltage and HV monitoring. The PMT voltages can be set and monitored by the control system [20,21]. The total power consumption of the OM is about 6 W. The PMT signals are multiplexed in the central titanium sphere and sent to shore via the electro-optical cable.

4.7. Final assembly and testing

Once the OM is completely assembled and cabled, the interior and ground glass joint are carefully cleaned and a small dessicator box on the aluminum disk is filled with silica gel. The sphere is then flushed with dry nitrogen gas in a chamber, slightly below atmospheric pressure, and closed. A band of self-adhesive plastic insulating tape is placed around the joint to avoid any slippage during manipulation. The assembled OM is pressure tested once again at 400 Atm for 12 h under high voltage while the singles rate is continuously monitored: they are then transferred to a dark room for storage and final electrical testing.

Care is taken during mounting of the OMs on the titanium floors and during deployment to minimise any exposure to direct light.

5. Tests performed on the NESTOR PMTs and OMs

5.1. Laboratory tests on the PMTs

In order to ensure that all the PMTs, which are used in the NESTOR neutrino telescope meet the

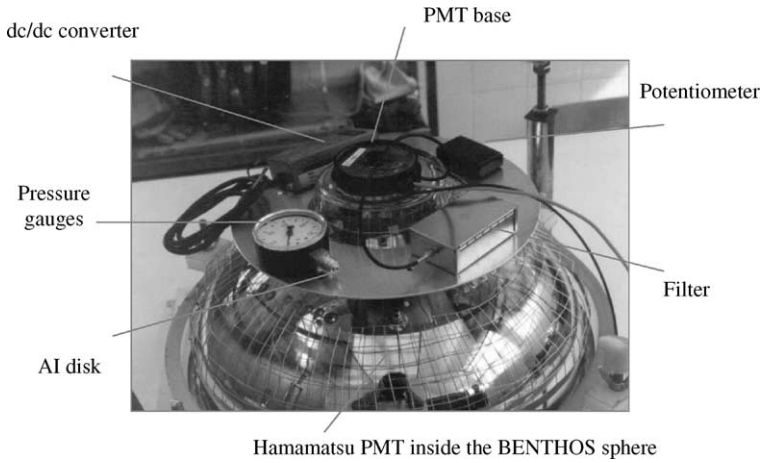

Fig. 6. The HV power supply and the divider were installed on an aluminum annular ring supported directly on the neck of the PMT.

specifications a series of quality control tests are performed on each PMT following delivery. Each PMT is set to a moderate voltage ($\sim$1700 V) and the output is examined to ensure that the pulse shape is correct.

Then the HV is set at a higher value ($\sim$2000 V) for at least 24 h. During this period its dark count rate is continuously monitored. This process takes place in a dark room where up to 60 PMTs can be tested simultaneously.

The measured dark count rate is typically below 10 kHz (at 30 mV threshold and 25°C), well below the 40 kHz maximum given in the manufacturer's specification. The measured pre-pulses[3] and late-/after-pulses[4] are below 2% and 3%, respectively, of the main pulses at the single photoelectron level. The temperature dependence of the dark count rate has been measured in a refrigerated enclosure (Fig. 7): As expected, the rate drops by more than a factor of two when the PMT is cooled from ambient temperature to 15°C, the ambient temperature inside the OM during operation in the sea [10].

Fig. 8 shows a typical noise pulse of the PMT R2018-03 at ambient temperature ($\sim$25°C). The pulse height is about 70 mV. The rise time is 7 ns and the FWHM $\approx$ 15 ns. The PMT's quantum efficiency, QE(λ) is presented as a function of wavelength in Fig. 9. The peak values, taken from the manufacturer's data sheets supplied with each PMT, are shown in Fig. 10. The mean value for the 223 PMTs that are being used is 19.59% at 390 nm.

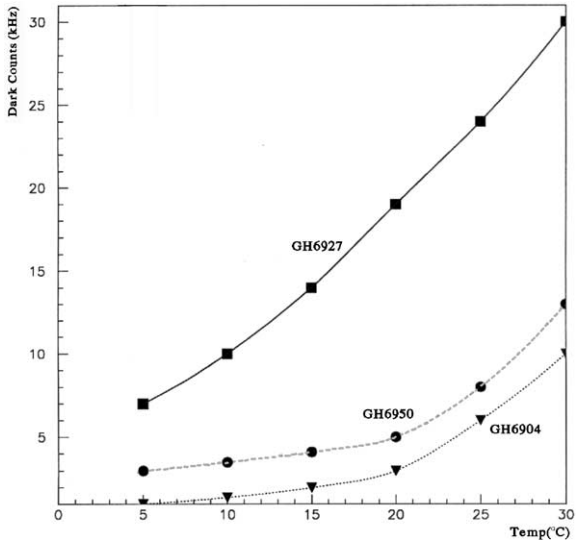

Fig. 7. The dark count rate of 3 PMTs is presented as a function of temperature.

[3] Pulses detected between 100 and 10 ns before the main pulse.

[4] Pulses detected between 10 and 100 ns after the main pulse (late-pulses). Pulses detected between 100 ns and 30 μs after the main pulse (after-pulses).

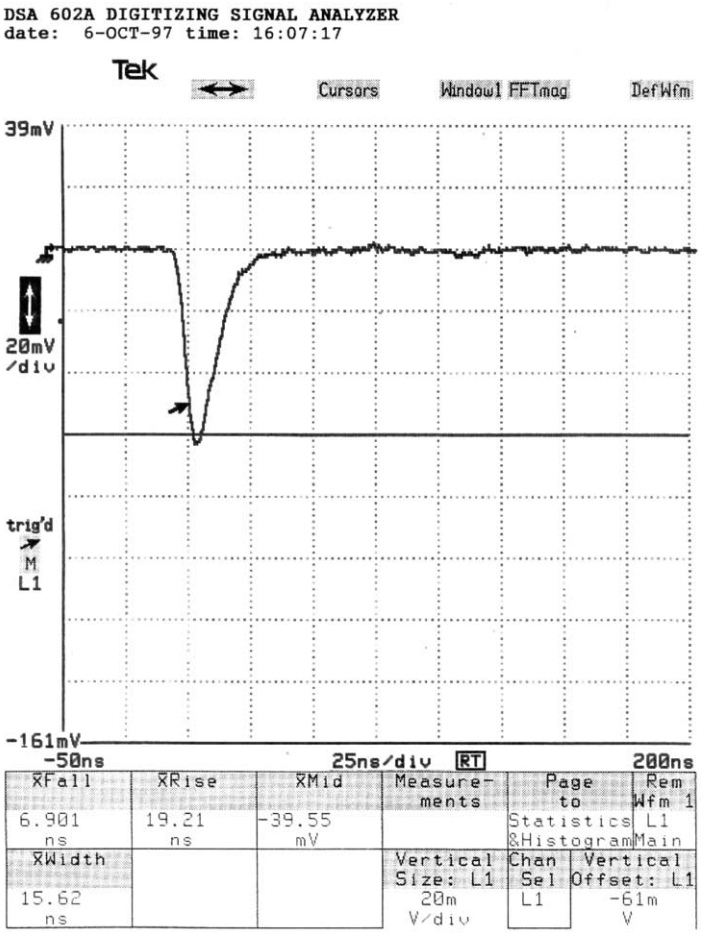

Fig. 8. A typical noise pulse of the PMT R2018-03.

In order to verify the performance of the PMT, the HV was set to give a gain 5×10^7 as specified by the manufacturer, and the following parameters were studied:

- The dark count rate,
- the peak to valley ratio at the single photoelectron level (pulse height distribution),
- the transit time spread (TTS) at the single photoelectron level,
- the uniformity of the photocathode (the response of the PMT measured as a function of the position of the incident light on the photocathode) at the multi-photoelecton level,
- the variation of TTS as a function of the number of the incident photons,
- the pre-, late- and after-pulse.

The variation of the gain as a function of the supplied voltage was also measured.

The test setup used is shown in Fig. 11. It consists of a light tight black box containing a mechanical stand, which holds the PMT within a grounded μ-metal cage. Two LEDs are attached at the end of an arm, controlled by stepping motors, which is able to rotate in θ and φ angles, thus covering the active surface of the PMT. The distance between the LEDs and the PMT is about

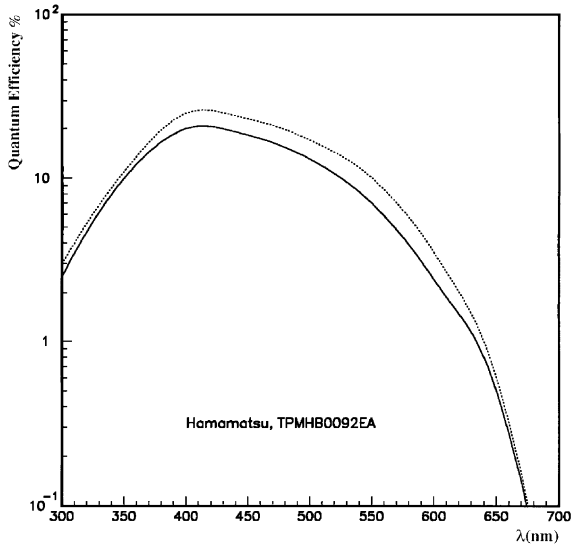

Fig. 9. The quantum efficiency of the PMT R2018-03 versus the wavelength. Due to the large size of the photocathode area a small decrease is noticed to the quantum efficiency in respect with the typical quantum efficiency of smaller PMTs (shown with dotted line).

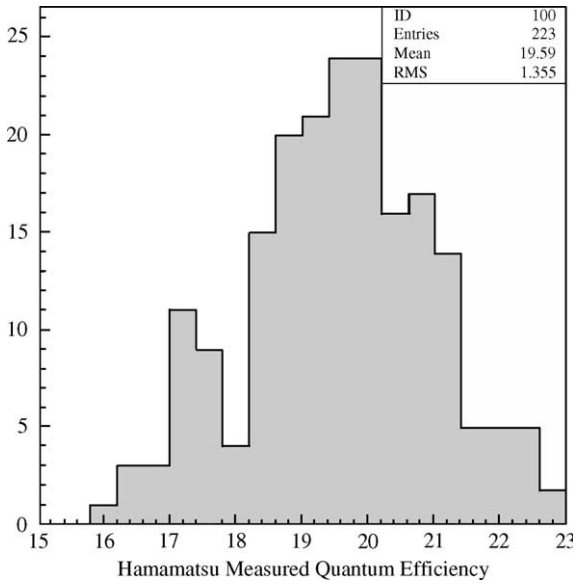

Fig. 10. The quantum efficiency of the 223PMTs that have been tested so far, as supplied by the manufacturer. The mean value is 19.59%.

2 cm. The amount of light emitted is controlled by sending pulses of known amplitude and duration to the selected LED. Two different pulse generators are used for this. The first, a pulser made by CAEN (Italy), is used to drive a LED at a variable pulse amplitude and duration for the multi-photoelectron level tests. The second pulser, made by Picosecond Inc. (Colorado, USA) gives pulse amplitude up to 50 V with a rise time of 0.5 ns; it drives a reverse biased LED in order to achieve single photoelectron conditions with accurate timing.

The system, including the HV supply and monitoring of the PMT, was operated from a CAMAC crate controlled by a PC. A block diagram of the DAQ system is shown in Fig. 12.

Fig. 13 shows a typical pulse height distribution at the single photoelectron level; the lower plot is a histogram of the peak-to-valley ratio[5] for the 223 PMTs measured. The peak obtained at the single photoelectron level is clearly visible above the dark count spectrum. The average peak-to-valley ratio is 1.5. In almost all cases it is better than the value of 1.2 given by the manufacturer.

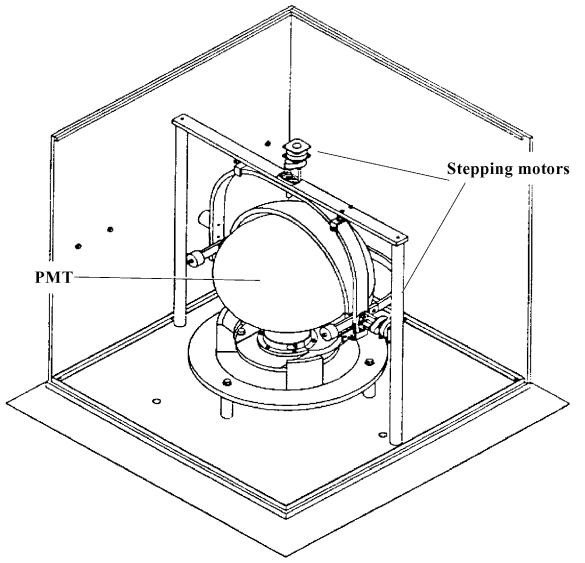

Fig. 11. The mechanical set-up used to test each PMT, showing the LED mounted upon a movable arm controlled by stepping motors.

[5] Peak-to-valley = (Number of entries at the peak of the distribution)/(Number of entries at the valley of the distribution). The two points are marked with arrows in Fig. 13.

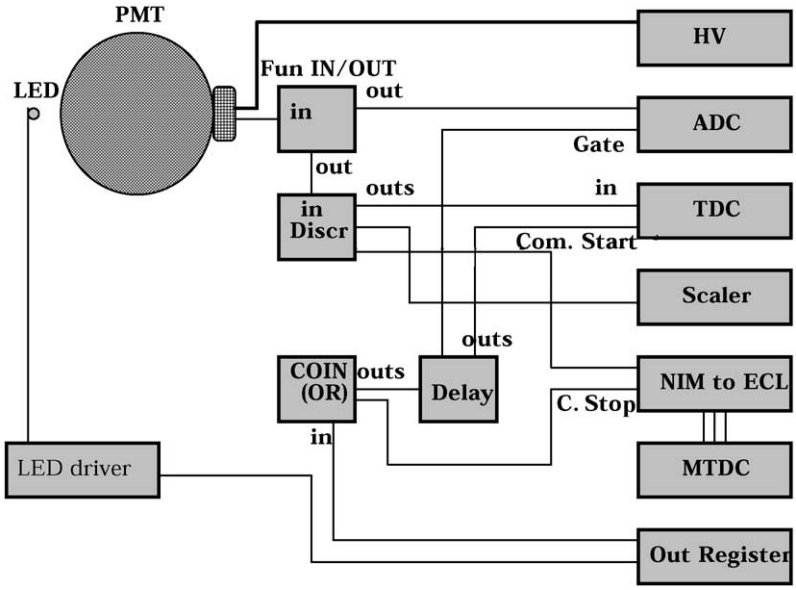

Fig. 12. The block diagram of the DAQ system used to test each PMT.

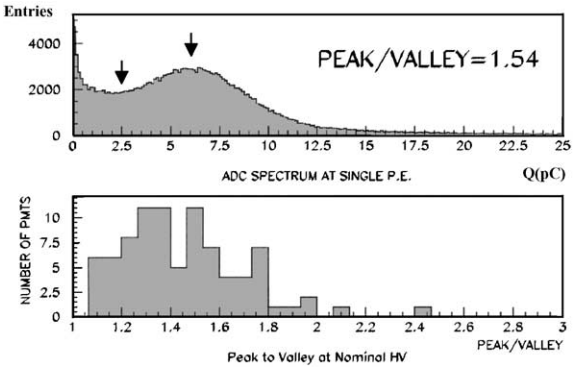

Fig. 13. A typical ADC spectrum at the single photoelectron level. The lower plot shows the peak-to-valley ratio for the 223 PMTs.

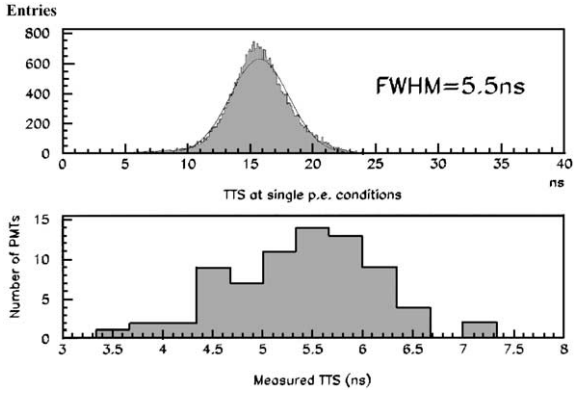

Fig. 14. The TDC spectrum at the single photoelectron level. The lower plot shows the TTS for the 223 PMTs.

Fig. 14 shows the transit time spread (TTS) obtained at the single photoelectron level for a typical PMT at nominal gain of 5×10^7 and a histogram of the values of the TTS of the 223 PMTs tested. The FWHM of the distribution is 5.5 ns, which compares well with the specifications. No PMT was accepted with FWHM greater than 7 ns. In Fig. 15 the TTS variation (slewing) as a function of the amplitude of the measured charge.

The surface of the photocathode was scanned with the LEDs. The time and pulse height response of each PMT was measured at 40 different points over the photocathode area in order to check its uniformity. For a randomly selected sample of PMTs (≈ 50) the scan was performed at 400 points. The variation of the PMT response as a function of the position of the incident light on the photocathode is shown in Fig. 16. It can be seen

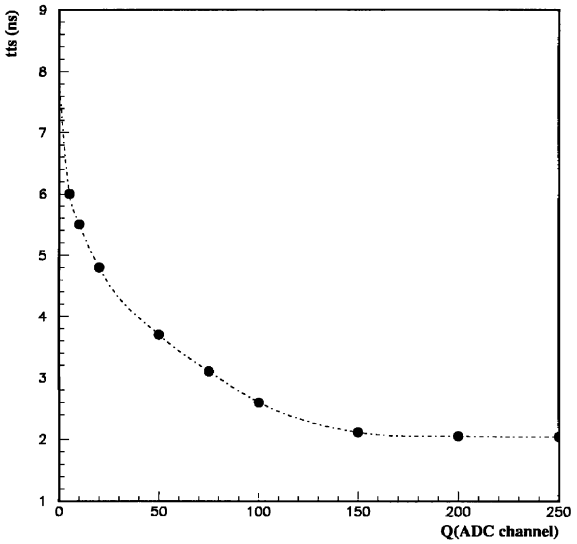

Fig. 15. The variation of TTS as a function of the amplitude of the registered charge.

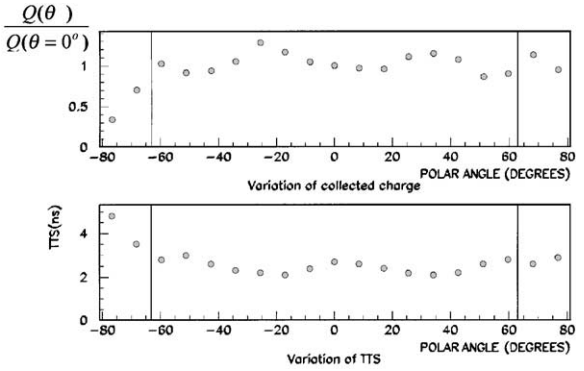

Fig. 16. The variation of PMT response as a function of the position of the incident light on the photocathode for one of the two vertical axes on which the scan was performed. These measurements are performed at the multi-photoelectron level.

that the PMT has a nearly uniform response inside the region of the photocathode ($\theta < 63^\circ$).

Tests have been performed to determine the linearity range of the NESTOR PMT. To test the linearity the LED was driven by a variable amplitude pulse. In Fig. 17 the PMT signal pulse height is plotted as a function of the amplitude of the LED driving pulse. The PMT signal displays a

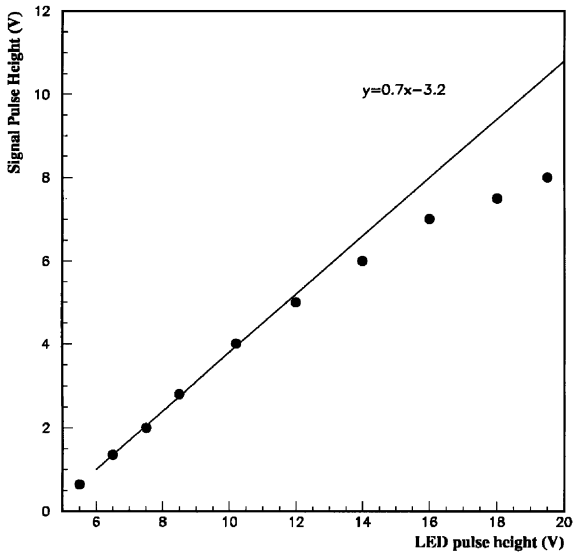

Fig. 17. The PMT signal pulse height as a function of the LED pulse amplitude.

good linearity for pulses up to 6 V, corresponding to about 50 photoelectrons.

5.2. Tests on the OMs response to muons

In order to study the response of the OM in near to final operating conditions, one OM was immersed in a water tank (built by the CEA, Saclay Laboratory, France) and placed in a muon beam at CERN, Geneva (M2 muon beam, 190 GeV). A diagram of the apparatus (Fig. 18) shows the layout and the hodoscopes used to define the direction of the incoming muon; measurements were also made using cosmic rays.

The water transmissivity was measured continuously with the use of an LED, placed on the top of the tank.

In Fig. 19, the OMs response is presented as a function of the distance d of the charged track from the center of the OM. For distances greater than 30 cm the number of photoelectrons is described with good agreement by the expression:

$$N_{\mathrm{pe}} = 50/\mathrm{d(m)}.$$

The angular dependence of the OMs response is presented in Fig. 20 for tracks at different distances from the OM. The polar dependence of the

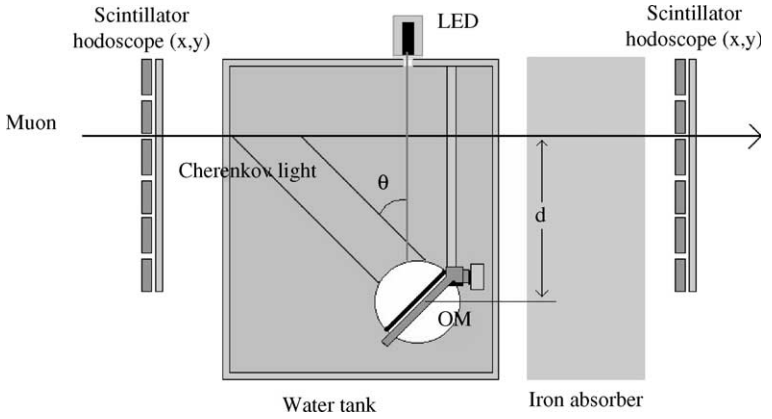

Fig. 18. Cross sectional view of the apparatus used for the test of the OMs.

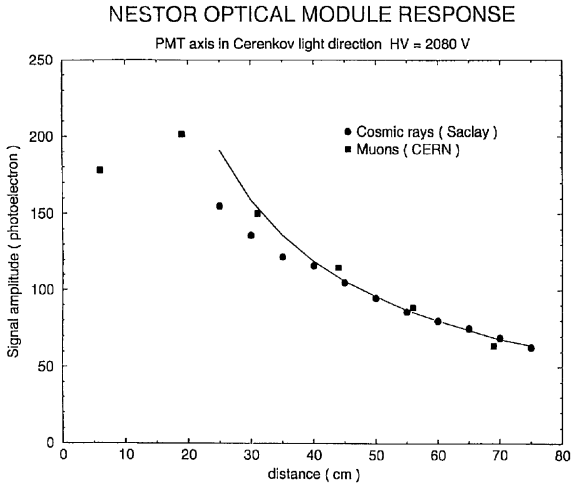

Fig. 19. The response of the OM versus the distance from the charged track. Note that tracks are crossing the OM for distances less than 20 cm (saturation for the track at 6 cm).

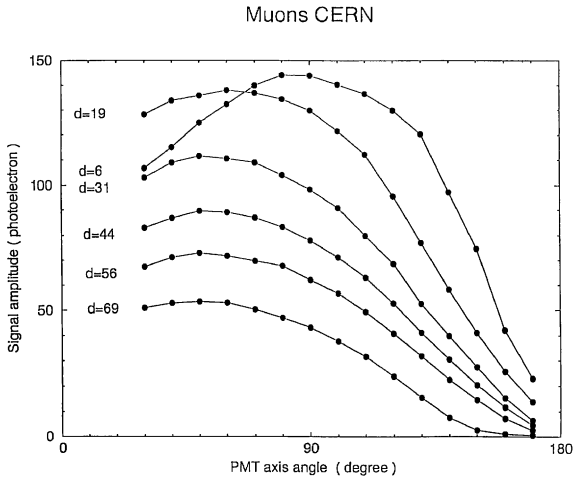

Fig. 20. The angular dependence of the OM's response for tracks at different distances.

sensitivity of the OM is approximately described by the formula (see Fig. 21):

$$S(\theta) = 0.525 + 0.475\cos\theta.$$

6. Calculation of the expected number of photoelectrons

In order to calculate the amount of light produced by relativistic, charged particle tracks in the vicinity of the detector, the number of Cherenkov photons produced in unit length of water at the Cherenkov angle is needed. The Cherenkov photons in the water per track length $\mathrm{d}l$ and wavelength $\mathrm{d}\lambda$ varies in inverse proportion to λ^2:

$$\frac{\mathrm{d}^2N}{\mathrm{d}l\,\mathrm{d}\lambda} = \frac{2\pi\alpha\sin^2\theta_c}{\lambda^2}$$

where

$$\sin^2\theta_c = 1 - \frac{1}{\beta^2 n^2(\lambda)} \quad \text{and} \quad \alpha = 1/137.$$

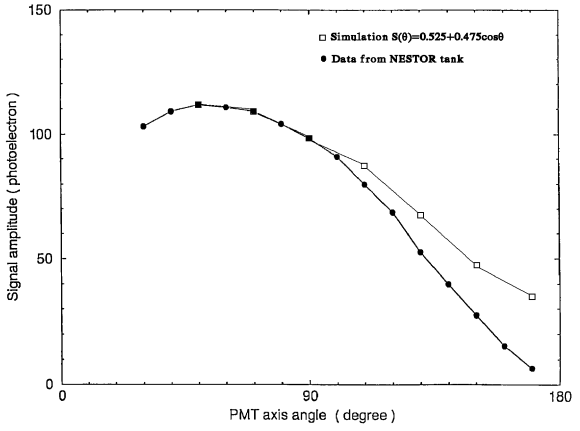

Fig. 21. The angular dependence of the OM's response for tracks at a distance of 31 cm is compared with the approximate formula $S(\theta) = 0.525 + 0.475\cos\theta$. For angles greater that 60° the agreement is not satisfactory. This is due to the fact the data were taken with the back hemisphere of the PMT covered while the simulation did not take this into account.

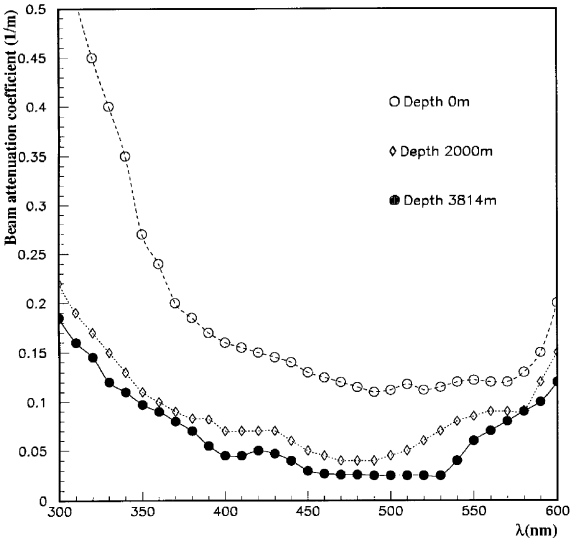

Fig. 22. The dependence of the attenuation coefficient of the water from the wavelength has been measured for different depths at the NESTOR site. The attenuation coefficient was measured to be $\beta = 0.018$ for $\lambda = 450$–530 nm at a depth of 3814 m.

The method used includes the following steps:

- The refractive index of seawater is expressed as a function of the wavelength; for this the average value of salinity, measured at the NESTOR site [10] has been used.
- The PMT's quantum efficiency, QE(λ) is also a function of wavelength (see Fig. 9). The peak values, taken from the manufacturer's data sheets supplied with each PMT, is shown in Fig. 10. The mean value of 19.59% at 390 nm has been used.
- The transparencies of the glass (BENTHOS housing and PMT envelope) and the gel or glycerin, $\mathrm{Tr}_{\mathrm{glass}}(\lambda)$ and $\mathrm{Tr}_{\mathrm{gel}}(\lambda)$ measured as functions of wavelength (see Fig. 5).

The resulting number of photons at a distance x from the track is given by

$$\frac{\mathrm{d}N}{\mathrm{d}l} = 2\pi\alpha \int_{\lambda\,\min}^{\lambda\,\max} \sin\theta_{\mathrm{c}} \frac{\mathrm{qe}(\lambda)\times \mathrm{ce} \times \mathrm{Tr}_{\mathrm{gl}}(\lambda)\times \mathrm{Tr}_{\mathrm{gel}}(\lambda)}{\lambda^2} \times \mathrm{e}^{-\beta(\lambda)x}\,\mathrm{d}\lambda$$

where ce is the collection efficiency of the PMT (see Section 2.1), while the exponential factor, $\mathrm{e}^{-\beta(\lambda)x}$ expresses the dependence of the attenuation coefficient of the water on the wavelength. The attenuation coefficient was measured to be $\beta = 0.018$ for $\lambda = 450$–530 nm (Fig. 22). The transmissivity of the seawater at NESTOR site is 55 ± 10 m [6].

The photons emitted by the track are distributed on a ring of radius $x\sin\theta$ and width $\sin\theta\,\mathrm{d}l$ so the density of photons per m^2 at a radial distance $\delta = x\sin\theta$ from the track is

$$\frac{\mathrm{d}N}{m^2} = \frac{\alpha}{\delta} \int_{\lambda\,\min}^{\lambda\,\max} \sin\theta_{\mathrm{c}} \frac{\mathrm{qe}(\lambda)\times \mathrm{ce} \times \mathrm{Tr}_{\mathrm{gl}}(\lambda)\times \mathrm{Tr}_{\mathrm{gel}}(\lambda)}{\lambda^2} \times \mathrm{e}^{-\beta(\lambda)x}\,\mathrm{d}\lambda.$$

Multiplying the above number by $0.108\,\mathrm{m}^2$, the projection of the surface of R2018-03 photocathode area, gives the number of photons seen by the PMT at radial distance δ from the track; Fig. 23 (curve 1). In the same plot, the data from the NESTOR water tank are indicated. Similar calculations by DUMAND (curve 2 for 30 m transmission length, curve 3 for 40 m transmission length) and data from their water tank tests are also shown [13]. Curve 4 shows a plot of the formula $N_{\mathrm{pe}} = 50/\delta(m)$ given previously as an approximation.

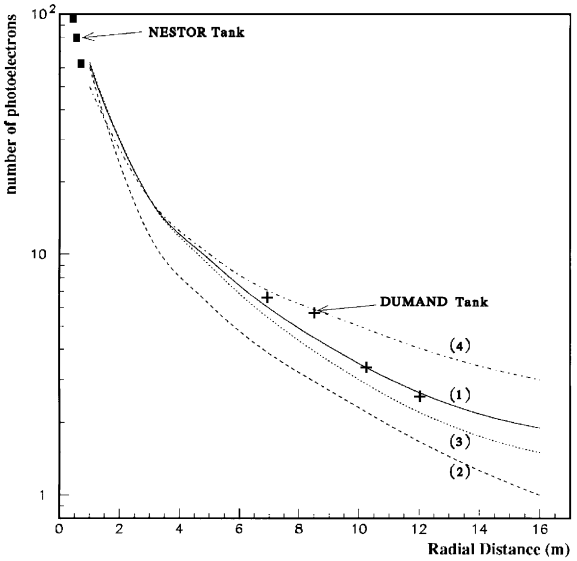

Fig. 23. The number of photons seen by the PMT at radial distance δ from the track according to the calculation presented above (1). In the same plot the data from the NESTOR water tank are presented. Similar measurements (DUMAND water tank) and calculations for different transmission lengths (2,3) are presented also. The approximate formula $N_{pe} = 50/\delta$ is plotted also as line (4), for reference.

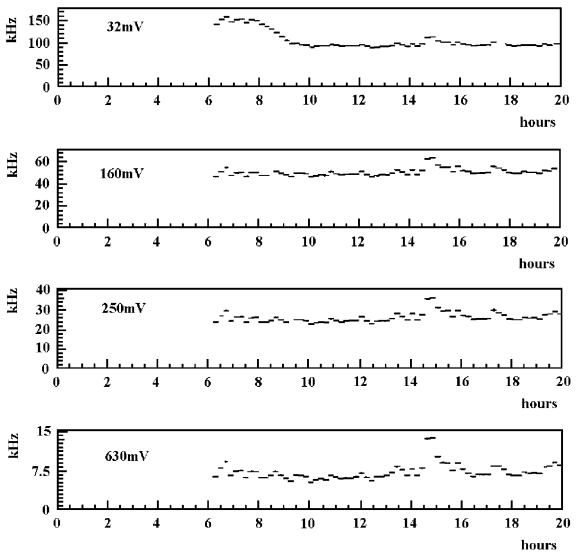

Fig. 24. The variation of the counting rate of an OM during operation at 3600 m depth for different discriminator thresholds.

7. Deep water tests

The NESTOR OMs have been used during test deployments (1996–2000). During these tests the optical background due to ^{40}K decay and bioluminescent activity was measured. In Fig. 24 the variation of the counting rate of an OM deployed in May 1996 at a depth of 3600 m is shown as a function of time for different discriminator thresholds. The counting rate of the PMTs due to ^{40}K has been measured to be about 70 kHz per PMT at the 0.25 photoelecton level [10]. Single rates of the PMTs at the same ambient temperature were 30 kHz.

In Fig. 25 the variation of the counting rate of two OMs, facing each other at a distance of 20 m is shown. This appears to be typical of bioluminescent activity. The duration of these events is not longer than 15 s while their frequency is about 20 per hour. In Fig. 26 two typical bursts detected by the second PMT are shown. The burst shows

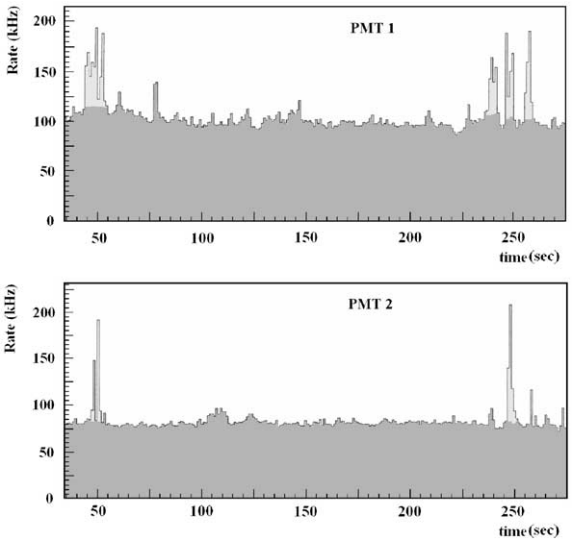

Fig. 25. The variation of the counting rate of two OMs during the same time interval, apparently due to bioluminescent activity.

a rapid increase followed by a decay. The duration of these particular events is not more than 5 s [10].

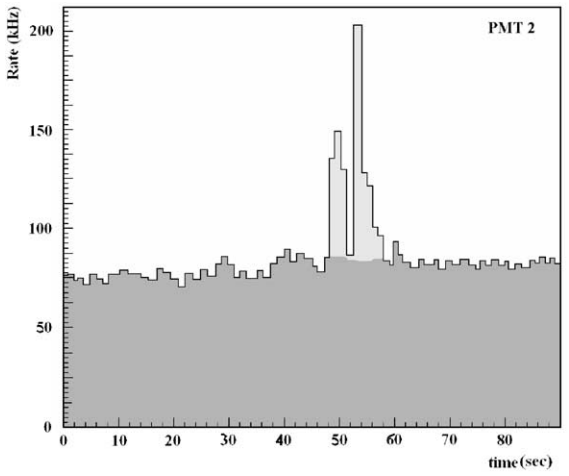

Fig. 26. Typical bursts measured by the second PMT due to the bioluminescent activity. The burst shows a rapid increase followed by an exponential decay. The background level is principally due to ^{40}K decay.

8. Conclusions

A sensitive and efficient OM has been developed for use in the NESTOR neutrino telescope. Tests of individual components and of the assembled module indicate long term reliability under demanding operating conditions. Parameters affecting the performance, such as the geomagnetic field and temperature inside the sphere during operation have been taken into consideration in the development. Background effects due to ^{40}K decay and bioluminescent activity have been evaluated.

The OM has been successfully tested both in the laboratory and in the sea down to 3800 m. The test and the calibrations have shown that the OMs have the ability to detect efficiently very small number of photons from Cherenkov radiation, thus allowing the detection and reconstruction of relativistic tracks of charged particles in the seawater at ranges of several tens of meters.

Acknowledgements

The authors wish to thank Captain M. Karpathakis and the crew of the OTE cable ship "THALES" as well as the Captain and crew of the 'Dynatos' for help and advice in numerous deployments. They also thank the staff in EST Division, CERN, Geneva for developing welding techniques and moulds for the production of the μ-metal cages and R. Grüb, ECP Division, CERN, for magnetic measurements of the prototypes. Measurements of the OM in water at the CERN muon beam were mainly carried out by staff from the CEA, Saclay, France who are now, no longer in the NESTOR collaboration. Our very sincere thanks are also due to all the technical staff from the collaborating institutes (in particular from the Universities of Athens and Kiel) who have participated in this work, for their unstinting efforts over several years.

Last, but not least, we greatly appreciate the cooperation of the Hamamatsu Photonics K.K. and Benthos Inc. throughout this project.

References

[1] L.K. Resvanis, in: V.J. Stenger, J.G. Learned, S. Pakvasa, X. Tata (Eds.), High Energy Neutrino Astrophysics, 1992 and NESTOR proposal NESTOR: A Neutrino Astroparticle Physics Laboratory for the Mediterranean, Vol. 1 & 2, 1995.
[2] L.K. Resvanis, Nucl. Instr. and Meth. A 433 (1999) 34.
[3] L.K. Resvanis, Proceedings of the second NESTOR International Workshop, Pylos, 1992.
[4] L.K. Resvanis, Proceedings of the third NESTOR International Workshop, Pylos, 1993.
[5] E. Anassontzis, et al., Nucl. Instr. and Meth. A 349 (1994) 242.
[6] S.A. Sotiriou, et al., (NESTOR collaboration), DESY-PROC-1999-01, July 1999.
[7] E. Trimonis, M. Rudenko, Nucl. Instr. and Meth. A 433 (1999) 321.
[8] V. Lykousis, et al., Submarine Power Link and Data Highway NESTOR/LAERTIS Cable Route Surveying. Morphological and Sedimentological Study, National Center for Marine Research, Athens, 1995.
[9] S. Katsanevas, et al., (NESTOR collaboration), Internal NESTOR Report, June 1996.
[10] S.A. Sotiriou, Ph.D. Thesis, University of Athens, Physics Laboratory, Athens, June 1998 (in Greek).
[11] M. Barone, et al., (NESTOR collaboration), Nucl. Phys. B (Proc. Suppl.) 61 (1998) 159.
[12] S. Matsuno, et al., Nucl. Instr. and Meth. A 276 (1989) 359;
C.M. Alexander, et al., (DUMAND Collaboration), DUMAND-2-93.

[13] H. Hanada, et al., A Highly Sensitive Optical Detector for a Use in Deep Underwater, Elsevier Preprint, 1996.
[14] S. Tanaka, A. Yamaguchi, Proceedings of the Dumand Optical Module Workshop, Sendai, Japan, 1990.
[15] G.R. Humphrey, Oceanographic Spherical Glass Instrumentation Housing, US patent #3, 587, 122, 1971.
[16] A.O. Deyneko, et al., The Tests of a Prototype of an Autonomous Module of Deep Underwater Neutrino Telescope during October–December 1989. Optimum Construction of an Autonomus Module, Moscow, P-700, 1991.
[17] I.A. Belolaptikov, et al., (Baikal collaboration), Astropart. Phys. 7 (1997) 263.
[18] B.K. Lubsandorzhiev, et al., (Baikal collaboration), I.C.R.C. (1997) HE 6.2.2.
[19] R.I. Bagduev, et al., (Baikal collaboration), Nucl. Instr. and Meth. A 420 (1999) 138.
[20] A. Capone, et al., (NESTOR collaboration), I.C.R.C. (1997) HE 4.1.18.
[21] L. Trassati, et al., NESTOR internal Report, NESTOR-LNF/2, 1996.